Engineering Geology 249 (2019) 60–70

Contents lists available at ScienceDirect

Engineering Geology

journal homepage: www.elsevier.com/locate/enggeo

DEM analyses of rock block shape effect on the response of rockfall impact against a soil buffering layer

Weigang Shen[a], Tao Zhao[b,c,*], Feng Dai[a], Mingjing Jiang[d], Gordon G.D. Zhou[e]

[a] State Key Laboratory of Hydraulics and Mountain River Engineering, College of Water Resource and Hydropower, Sichuan University, Chengdu 610065, China
[b] Formerly at State Key Laboratory of Hydraulics and Mountain River Engineering, College of Water Resource and Hydropower, Sichuan University, Chengdu 610065, China
[c] Department of Civil and Environmental Engineering, Brunel University London, London UB8 3PH, United Kingdom
[d] Department of Civil Engineering, Tianjin University, Tianjin 300072, China
[e] Institute of Mountain Hazards and Environment, Chinese Academy of Sciences & Ministry of Water Conservancy, Chengdu, China

ARTICLE INFO

Keywords:
Rockfall
Soil buffering layer
Discrete element method
Rock block shape

ABSTRACT

This study investigates the mechanism of rockfall impact against a granular soil buffering layer above a concrete/rock shed via numerical simulations by discrete element method (DEM). The soil buffering layer is modeled as a loose packing of polydisperse spherical particles, while the bottom concrete/rock shed is simulated by a layer of fixed particles. The rock blocks of various ellipsoidal shapes are represented by an assembly of densely packed and bonded spherical particles. The DEM model was employed to investigate the dynamic interaction between the rock block and the soil buffering layer, including the impact force, penetration depth and bottom force. During the rockfall impact, the force chains occur immediately at the impact area and then propagate radially downward into the soil buffering layer. The force waves vanish gradually as most of the impact energy was absorbed and dissipated by the loose buffering soil particles. The numerical results show that the maximum impact force acting on the rock block increases, while the corresponding penetration depth decreases linearly with the block sphericity. The maximum force acting on the bottom concrete/rock shed is approximately twice the maximum impact force acting on the rock block, showing apparent force amplification of the soil buffering layer. The ratio between these two forces is almost independent of the rock block sphericity. These findings can finally contribute to the design of effective soil buffering layer for concrete/rock sheds.

1. Introduction

Rockfall is a type of natural hazard that involves detachment of rock blocks from a steep slope or cliff, followed by rapid downslope movements as characterized by freefall, bouncing, rolling and sliding (Cruden and Varnes, 1958; Ferrari et al., 2016). It can pose significant hazards to human lives, infrastructures and lifeline facilities worldwide due to the high kinetic energy and undefined trajectory (Dorren, 2003; Crosta and Agliardi, 2004; Agliardi et al., 2009; Valagussa et al., 2014). To mitigate the rockfall impact, protection structures such as reinforced concrete/rock sheds, retaining walls, rigid/flexible barriers and embankments have been widely constructed in mountainous areas (Volkwein et al., 2011; Lambert and Bourrier, 2013). Among others, the concrete/rock shed plays an important role in protecting highways along steep slopes from rockfall impacts. It is generally composed of a base reinforced concrete roof slab and a granular buffering layer (usually soil and gravels). The soil buffering layer can effectively absorb and dissipate the impact energy of falling rock blocks, and thus reduce the maximum impulsive force acting on the concrete/rock shed.

The design of a concrete/rock shed requires proper estimations of rock block penetration depth into the soil buffering layer and the dynamic impulsive forces generated during the impact. Up to now, several empirical methods have been developed to estimate these forces in engineering practice, such as the Chinese, Japanese and Swiss design codes (*Ministry of Transport of the People's Republic of China*, 1995; Japan Road Association, 2000; ASTRA, 2008). Even though these methods are simple and easy to use in practice, none of them have been acknowledged as a universal code to calculate the impact forces, because each method was obtained in specific impact and boundary conditions. Thus, attempts to reconcile the detailed impact process of rock blocks against a soil buffering layer and the corresponding mechanical response of the concrete/rock shed are still needed.

* Corresponding author at: Department of Civil and Environmental Engineering, Brunel University London, London, UB8 3PH, United Kingdom.
E-mail addresses: wgshen@stu.scu.edu.cn (W. Shen), tao.zhao@brunel.ac.uk (T. Zhao), fengdai@scu.edu.cn (F. Dai), mingjing.jiang@tju.edu.cn (M. Jiang), gordon@imde.ac.cn (G.G.D. Zhou).

https://doi.org/10.1016/j.enggeo.2018.12.011
Received 16 July 2018; Received in revised form 16 December 2018; Accepted 17 December 2018
Available online 23 December 2018

The dynamic interaction between a rock block and a soil buffering layer is complicated because it depends on the properties of rock blocks (e.g. mass, shape and impact velocity), the geometrical characteristics of the soil buffering layer (e.g. density, thickness) and the mechanical properties of soil (e.g. grains shape, stiffness and friction) (Labiouse et al., 1996). Among these factors, the influences of buffering soil thickness, block mass and velocity on the rockfall impact process have been investigated intensively (Labiouse et al., 1996; Calvetti and di Prisco, 2012; Breugnot et al., 2016). In these studies, researchers usually consider the rock block as a rigid sphere or cylinder. In fact, the shape of real rock block can vary significantly from sphere, cone, cylinder to disc (Fityus et al., 2013), which can influence the rockfall dynamics significantly (Leine et al., 2014; Glover et al., 2015; Gao and Meguid, 2018a; Gao and Meguid, 2018b). Degago et al. (2008) used semispherical and pyramidal rock blocks in small scale rockfall impact experiments. Their results indicate that the geometry of rock block has a significant influence on the magnitude of impact force and penetration depth. Through experimental and numerical analyses, Pichler et al. (2005) established functional relationships between the targeted quantities of rockfall (i.e. impact force, penetration depth and duration time) and the block properties (i.e. mass, velocity and soil indentation resistance). However, their approach only analyzed a simple case of cubic rock block shape.

According to Glover (2015), although advancements exist, detailed investigations of block shape effect on the mechanical response of rockfall impact against a soil buffering layer are still needed. In recently years, the discrete element method (DEM) (Cundall and Strack, 1979) has become a proper numerical tool for analyzing rockfall impact from the micro- to macroscopic scales. With proper calibrations against the well-documented experimental data, DEM allows researchers to analyze some quantities that are nearly impossible to obtain by experiments. Zhang et al. (2017a) employed a three-dimensional DEM model to investigate the energy propagation and block bouncing during rock block impact on a granular medium. Bourrier et al. (2010) and Zhang et al. (2017b) investigated the evolution of impact induced force chains and its relation to the global mechanical response of the granular buffering layer by DEM. Calvetti et al. (2005) studied the impact of a block on a shelter covered by a soil buffering layer using the commercial three-dimensional DEM software PFC3D. The initial kinetic energy of falling block was set as 5000 kJ. Such a high impact energy is generally not investigated in experiments to avoid the potential damages of measurement devices (e.g. loading cells). Roethlin et al. (2013) used a three-dimensional DEM model to study the stress distribution on a concrete slab. In these tests, the DEM has been found to be an effective method to investigate the impact response of a soil buffering layer.

In the present study, the mechanical responses of rockfall impact against a soil buffering layer have been investigated by discrete element modeling. The paper is organized as follows: Section 2 presents a brief introduction of the DEM model. Section 3 performs DEM model validation and a parametric study of rock block sphericity. Section 4 discusses the importance of rock shape effect in engineering design of concrete/rock sheds. Finally, some conclusions on the capability of DEM to model the rockfall impact process are provided in Section 5.

2. DEM theory and model configurations

2.1. DEM theory

The open source DEM code ESyS-Particle (Weatherley et al., 2014) was employed to run all the simulations presented herein. This model has been widely used to analyze the mechanical behavior of solids (e.g. soil and rock) during rockfalls and debris flows (Zhao et al., 2017; Shen et al., 2018; Zhao et al., 2018). In DEM, the granular materials are modeled as a collection of rigid spherical particles. The translational and rotational motions of each particle are governed by the Newton's second law of motion as:

$$F_i = m_i \frac{d^2}{dt^2}\boldsymbol{r_i} \tag{1}$$

$$M_i = I_i \frac{d^2}{dt^2}\boldsymbol{\omega_i} \tag{2}$$

where F_i is the resultant force acting on particle i; $\boldsymbol{r_i}$ is the position of its centroid; m_i is the particle mass; M_i is the resultant moment acting on the particle; $\boldsymbol{\omega_i}$ is the angular velocity and I_i is the moment of inertia.

The interactions between particles can be evaluated by the linear elastic spring-dashpot and parallel bond models for frictional and bonded contacts, respectively (Itasca, 2003; Potyondy and Cundall, 2004). In the frictional particle contact, the normal contact force (F_n) is calculated as,

$$F_n = k_n u_n + F_n^d \tag{3}$$

where u_n is the overlapping distance between the two particles in contact; k_n is the normal contact stiffness and $F_n{}^d$ is the normal damping force.

The normal contact stiffness is defined as,

$$k_n = \pi E(R_A + R_B)/4 \tag{4}$$

where E is the particle Young's modulus; R_A and R_B are the radii of the two particles.

The normal damping force ($F_n{}^d$) is used to replicate energy dissipation by plastic deformation of particles in the normal direction of contact, which can be calculated as,

$$F_n^d = -2\beta\sqrt{0.5(m_A + m_B)k_n}v_n \tag{5}$$

where β is the damping coefficient; m_A and m_B are the mass of the two particles; v_n is the relative velocity between particles in the normal direction.

The shear force at the current time step (F_s^n) is calculated incrementally as,

$$F_s^n = F_s^{n-1} + (\Delta F_{s1} + \Delta F_{s2}) \tag{6}$$

where $F_s{}^{n-1}$ is the shear force at the previous iteration time step. ΔF_{s1} is calculated as $k_s \Delta u_s$ with k_s being the shear contact stiffness and Δu_s being the incremental shear displacement. The shear stiffness is calculated as $k_s = \pi E(R_A + R_B)/(8(1 + \upsilon))$ with υ being the particle Poisson's ratio. ΔF_{s2} is the shear force related to the rotation of particle contact plane. A detailed description of these two shear force terms can be found in Wang and Mora (2009).

The magnitude of the shear force is limited by the Coulomb's law of friction as,

$$|F_s| \le \mu\ |F_n| \tag{7}$$

where μ is the friction coefficient of particle contact.

The shear induced moment is computed as:

$$M = F_s \boldsymbol{r_i} \tag{8}$$

The interactions between bonded particles are calculated after Wang (2009) as:

$$F_{bn} = k_{bn} \cdot \Delta l_n \tag{9}$$

$$F_{bs} = k_{bs} \cdot \Delta l_s \tag{10}$$

$$M_b = k_b \cdot \Delta\alpha_b \qquad M_t = k_t \cdot \Delta\alpha_t \tag{11}$$

where F_{bn}, F_{bs} are the normal and shear bonding forces; M_b and M_t are the bending and twisting moments, respectively. $k_{bn} = \pi E_b l_0/4$, $k_{bs} = \pi E_b l_0/(8(1 + \upsilon))$, $k_b = \pi E_b {l_0}^3/64$ and $k_t = \pi E_b {l_0}^3/(64(1 + \upsilon))$ are the corresponding bonding stiffness in the normal, shear, bending and twisting directions, with E_b being the Young's modulus, υ being the Poisson's ratio of the bond. l_0 is the initial distance between particle centers. Δl_n, Δl_s, $\Delta\alpha_b$ and $\Delta\alpha_t$ are the relative displacements between the bonded particles in the normal, shear, bending and twisting directions with respect to the initial particle positions.

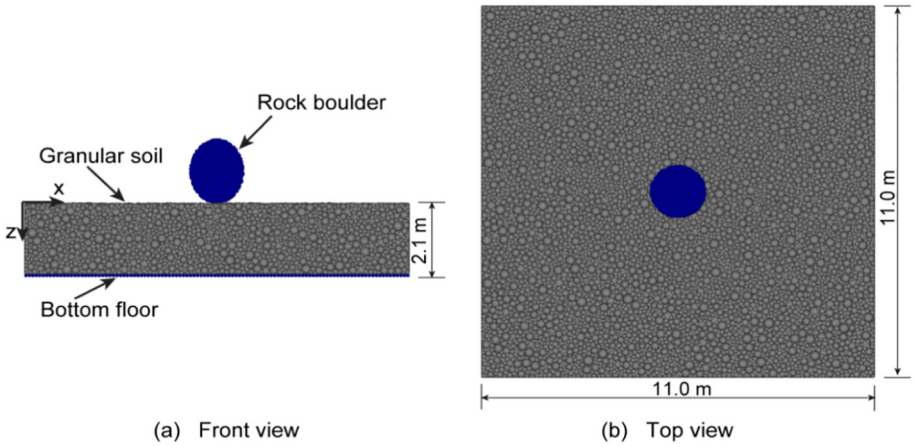

Fig. 1. Numerical model configurations (a) front view; (b) top view. The rock boulder is modeled as an assembly of bonded spherical particles, and the buffering layer is modeled as an assembly of polydisperse spherical particles obtained by gravitational deposition.

The criterion of bond breakage is determined as follows:

$$\frac{F_{bn}}{F_{bnMax}} + \frac{F_{bs}}{F_{bsMax}} + \frac{M_b}{M_{bMax}} + \frac{M_t}{M_{tMax}} \geq 1 \tag{12}$$

where F_{bnMax}, F_{bsMax}, M_{bMax} and M_{tMax} are the maximum normal and shear bonding forces, bending and twisting moments, respectively. They can be calculated as $F_{bnMax} = \pi c {l_0}^2/4$, $F_{bnMax} = \pi c {l_0}^2/4$, $M_{bMax} = \pi c {l_0}^3/32$ and $M_{tMax} = \pi c {l_0}^3/16$, with c being the cohesive strength of the particle bond. In the present study, c is set to an extremely high value (e.g. 10^{20} MPa) to avoid the fragmentation of rock block.

2.2. DEM model configurations

The DEM model configurations of rockfall impact against a soil buffering layer are shown in Fig. 1.

In this model, the concrete/rock slab is represented by a layer of fixed particles with radii of 0.05 m, hereafter called the “bottom”. The soil buffering layer is modeled as an assembly of polydisperse cohesionless rigid spherical particles. Thus, the damage or fragmentation of the soil particles is not considered in this study. The soil buffering layer is confined by four lateral walls and the bottom. The soil buffering layer is 2.1 m in thickness, 11.0 m in length and width, respectively (see Fig. 1).

The falling rock block is modeled as a rigid sphere or ellipsoid (see Fig. 2) which consists of a collection of densely packed and bonded spherical particles. To quantitatively describe the overall rock block shape, the sphericity index (S_p) is employed. According to Krumbein (1941), S_p is defined as,

$$S_p = \sqrt[3]{D_2 \cdot D_3 / D_1^2} \tag{13}$$

where D_1, D_2 and D_3 are the longest, intermediate and shortest diameters of an ellipsoid, respectively. The geometrical parameters of four different blocks used in this study are also labeled in Fig. 2. The mass of all the blocks is fixed as 5410.6 kg by varying the density of individual particles in the rock block (see Table 1).

The input parameters of the DEM model are listed in Table 1. The Poisson's ratio, coefficient of friction, particle Young's modulus and density are set according to the commonly used values in numerical simulations of granular media (Bourrier et al., 2008; Utili et al., 2015). During the simulation, gravitational deposition of particles in the soil buffering layer is firstly performed by applying gravitational forces to all soil particles until the total kinetic energy of the system becomes nil. After the gravitational deposition, the bulk density of the granular layer is measured as 1514.9 kg/m^3. Then, the rock block is positioned in the middle and just above the surface of the soil buffering layer. The initial impact velocity (v_0) of the rockfall impact is set translationally and vertically down according to the aimed falling height h_f (i.e. $v_0 = \sqrt{2gh_f}$), as shown in Table 2. The impact velocities are chosen according on the well-documented values reported in the literature (Calvetti et al., 2005; Calvetti and di Prisco, 2012). To simplify the analysis, the rotational velocity and incident impact angle of a rock block have been ignored. Though, these two factors can be very influential to the impact process, they are not within the purview of the current study for a preliminary analysis. In this study, each simulation lasts around 24 h on a standard desktop computer (Intel® Core™ i7 CPU, 4.00 GHz × 8, and 16 GB RAM).

3. Numerical results

As a preliminary study, the spherical block is firstly used in the rockfall simulation (Sections 3.1) as a model validation against some well-documented experimental and numerical investigations of similar model configurations in the literature (Calvetti and di Prisco, 2012; Zhang et al., 2017a). Then, the dynamics and the influence of rock block shape on the rockfall impact process will be investigated with respect to the impact forces and penetration depth (Sections 3.2–3.6).

3.1. DEM model validation

To validate the DEM model, a series of simulations were conducted under conditions of various falling heights (h_f). In these simulations, the rock block is modeled as a rigid sphere with diameter of 0.9 m and mass of 850 kg to match those used in Calvetti and di Prisco (2012). The focus is to analyze the impact force on the rock block (F_{boul}), the vertical contact force between the soil buffering layer and the bottom floor (F_{bott}), and the penetration depth (Z_{boul}), as shown in Fig. 3 (a). In the analyses, F_{boul} is calculated as the sum of vertical contact forces acting on the rock block. The bottom force at time t is calculated as $F^t_{bott} = F^t_c - F^{t_0}_c$, with F^t_c and $F^{t_0}_c$ being the normal component of total contact force acting on the bottom floor at time t and t_0 (0 s), respectively. Note that $F^{t_0}_c$ is equal to the gravity of the soil buffering layer. The penetration depth at time t is calculated as $Z^t_{boul} = Z^t - Z^{t_0}$, with Z^t and Z^{t_0} being the heights of the block centroid relative to the surface of soil buffering layer at t and t_0, respectively.

As shown in Fig. 3 (a), F_{boul} increases immediately during the impact and reaches the maximum value of 2.49×10^6 N quickly at 0.002 s. Then, it decreases gradually to zero at $t_b = 0.042$ s. When compared to the impact force, F_{bott} exhibits a time-delayed evolution pattern. It remains constant as zero during t = 0.0–0.0092 s, because it takes time for the impact induced force wave to propagate from the surface to the bottom of the soil buffering layer. The average wave

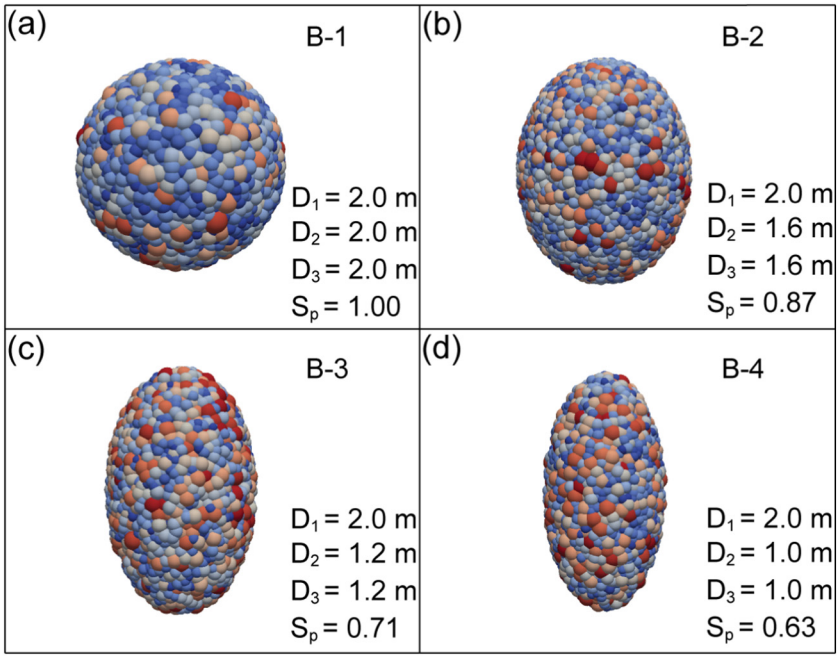

Fig. 2. Different rock blocks (B-1, B-2, B-3 and B-4) used in the simulations. D_1, D_2 and D_3 are the longest, intermediate and shortest diameter, respectively. S_p is the sphericity of a rock block calculated as $S_p = \sqrt[3]{D_2 \cdot D_3 / D_1^2}$.

propagation velocity (v_p) can be computed simply as the layer thickness divided by the propagation time (t_a) ($v_p = H/t_a$). The obtained velocity is 228 m/s which is close to the experimental ones found in Calvetti and di Prisco (2012) (ca. 250–300 m/s) and the numerical results in Zhang et al. (2017a) (~ 227 m/s). After $t_a = 0.0092$ s, F_{bott} increases quickly to the peak value of 4.03×10^6 N, and then decreases gradually to be negative. Here, the negative value indicates that the bottom force is smaller than its initial value (i.e. gravity of soil buffering layer) due to the rebound of soil particles from the bottom. This phenomenon has also been observed by Calvetti and di Prisco (2012) in their experimental studies. In the current DEM modeling, the particle rebound during impact can be easily investigated by tracking the number of soil particle contacts (N_{bc}) with the bottom floor. According to Fig. 3 (b), N_{bc} evolves similarly as the bottom force. Between 0 to t_a, N_{bc} remains a constant value of 5421 as determined by the initial packing state. After t_a, N_{bc} increases slightly due to soil compaction by force waves reaching the bottom. Then, the reflected force waves trigger the rebound of soil particles from the bottom floor, and N_{bc} decreases gradually to the minimum value of 4589. This reduction of N_{bc} indicates the separation of soil particles from the bottom floor.

In Fig. 3 (a), it can be seen that the maximum value of F_{bott} (F_{bott}^{max}) is much larger than that of F_{boul} (F_{boul}^{max}), indicating that the numerical model can effectively reproduce the dynamic amplification of impact force as observed in some well-documented experimental studies (Labiouse et al., 1996; Calvetti et al., 2005; Lambert et al., 2009; Calvetti and di Prisco, 2012). In this study, the obtained amplification ratio is 1.6 which is very close to the experimental and numerical values reported in Stoffel (1998) and Zhang et al. (2017a).

Table 2
Initial vertical velocity of rockfall impact.

Vertical velocity, v_0 (m/s)	Equivalent falling height, h_f (m)
10.0	5.1
15.0	11.5
20.0	20.4
30.0	45.9

The numerical results for tests of various falling heights are compared with the experimental data in Calvetti and di Prisco (2012), with regard to the maximum impact force (F_{boul}^{max}) and penetration depth (Z_{boul}^{max}) (see Fig. 4 (a) and (b)). It can be seen that F_{boul}^{max} is overestimated, while Z_{boul}^{max} is underestimated in the current numerical study. This is because the rigid spheres are employed to represent the soil particles in the DEM model, which would exert higher resistance on the rock block than the real soil (Zhang et al., 2017a). However, the evolution of numerical results can follow well the trend of experimental results. In both numerical and experimental studies, F_{boul}^{max} and Z_{boul}^{max} increase with the equivalent falling height following power law relationships as,

$$F_{boul}^{max} = F_0 (h_f/h_0)^{\beta} \quad (14)$$

$$Z_{boul}^{max} = Z_0 (h_f/h_0)^{\gamma} \quad (15)$$

Table 1
Input parameters used in the simulations.

DEM parameters	Value	DEM parameters	Value
Soil particle radius, r (m)	0.05–0.15	Young's modulus of particle, E_p (MPa)	1×10^2
Slab particle radius, r_s (m)	0.05	Particle Poisson's ratio, υ	0.25
Block particle radius, r_b (m)	0.03–0.06	Viscous damping coefficient, β	0.01
B-1 particle density, ρ_{B1} (kg/m^3)	2650.0	Particle friction coefficient, μ	0.577
B-2 particle density, ρ_{B2} (kg/m^3)	4210.3	Cohesion of bonds, c (MPa)	1×10^{20}
B-3 particle density, ρ_{B3} (kg/m^3)	7559.6	Young's modulus of bonds, E_b (MPa)	1×10^4
B-4 particle density, ρ_{B4} (kg/m^3)	10,986.4	Gravitational acceleration, g (m/s^2)	9.81
Soil particle density, ρ (kg/m^3)	2650.0	Time step size, Δt (s)	1×10^{-6}

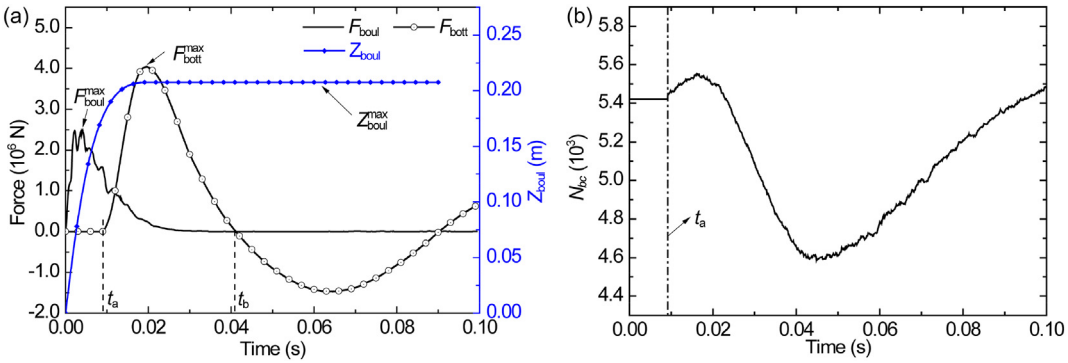

Fig. 3. (a) Evolutions of the impact force (F_{boul}), the bottom force (F_{bott}) and penetration depth (Z_{boul}) for the test of h_f = 40.0 m. Z_{boul} = 0.0 corresponds to the initial height of rock block centroid relative to the surface of soil buffering layer. (b) Evolution of the number of soil particles contacting with the bottom floor. In the figure, t_a = 0.0092 s and t_b = 0.042 s.

where F_0, Z_0 and h_0 are constants of the power law fitting; β and γ are the fitting coefficients.

Although the fitting constants are different for the numerical and experimental results, the coefficients β and γ are the same in both cases. This indicates that the power law relationship can well describe the dependence of F^{max}_{boul} and Z^{max}_{boul} on the falling height for the rockfall impact tests with similar model configurations. The well-match of numerical results with the experimental observations illustrates that the numerical model can effectively reproduce the general response of soil buffering layer against the rockfall impact, with respect to the maximum impact force, penetration depth, the force wave propagation and amplification. This confirms the applicability of DEM model to investigate the mechanical response of block impact against a soil buffering layer. In the following sections, the validated DEM model is used to investigate the influences of rock block shape and impact velocity (see data in Fig. 2 and Table 2) on the induced forces and penetration depth.

3.2. Dynamics of rockfall impact by a spherical block

Fig. 5 illustrates the dynamic impact process of a spherical rock block (B-1) into a soil buffering layer at h_f = 11.5 m. For visualization purpose, the soil buffering layer has been divided into four equal-sized sub-layers (i.e. S-1, S-2, S-3 and S-4) with distinct colors at a time instant just before the impact (see Fig. 5 (a)). According to Fig. 5, during impact, the rock block gradually penetrates the granular layer. Particles beneath the rock block are pushed to move downward, while the surrounding particles move laterally, forming a bowl-shaped crater (Fig. 5 (c)-(e)). The maximum penetration depth of the block is 0.22 m achieved after t = 0.24 s.

The corresponding compressive force wave propagation within the soil buffering layer can be represented by the evolution of force chains, as shown in Fig. 6. The force chains are defined as a network of straight lines connecting the centers of contacting particles. The thickness of these lines is proportional to the magnitude of normal contact force. According to Bourrier et al. (2008), the propagation of force chains within an assembly of granular materials can be used to quantify the propagation of compressive stress waves. From Fig. 6, it can be observed that during impact, a shock force wave propagates radially from the impact point downward within the soil layer (see Fig. 6 (b-f)). The large contact forces concentrate mainly beneath the rock block, while small contact forces distribute near the propagation front. After reaching the bottom floor at t = 0.02 s, the force chains propagate laterally affecting a much wider area (see Fig. 6 (d-e)). In this process, the distribution of force chain network exhibits a cone shape in space. After t = 0.025 s, the force chains begin to vanish as the block gradually cease motion, with only a small number of force chains persist near the bottom edge of rock block (see Fig. 6 (g) and (h)). In the end, no force chains exist in the soil buffering layer and the rock block reaches the maximum penetration depth (see Fig. 6 (i)).

Fig. 7 shows the evolutions of kinetic energy of the rock block ($E_k{}^b$), the kinetic ($E_k{}^l$) and strain ($E_s{}^l$) energy of the soil layer, and the energy loss due to soil particle friction ($E_f{}^l$) and damping ($E_D{}^l$). The calculation of each energy component can be found in our recent publication Shen et al. (2018). Here, all energy components are normalized by the initial kinetic energy of the rock block (E_0). As shown in Fig. 7, during impact, the normalized kinetic energy of the rock block ($E_k{}^b$) decreases, while the kinetic ($E_k{}^l$) and strain energy ($E_s{}^l$) of the soil buffering layer increase quickly, indicating that a majority of rockfall energy has been transferred into the soil buffering layer by the impact force chain

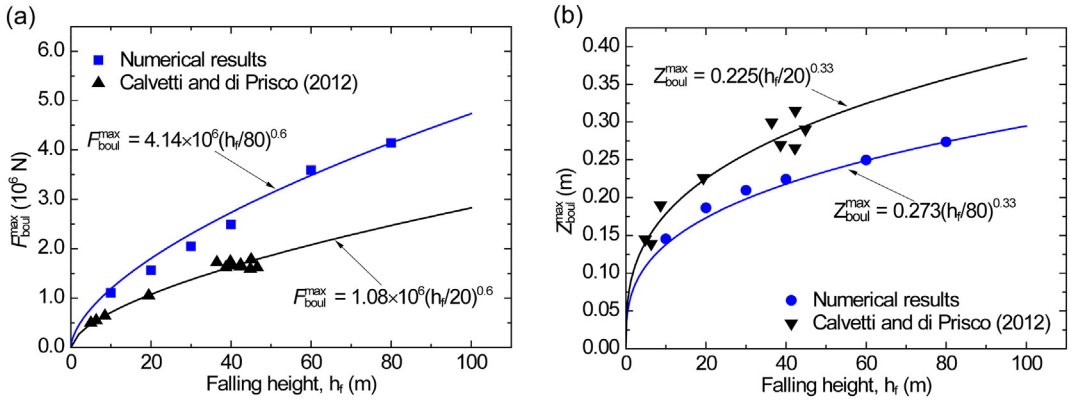

Fig. 4. Comparisons between the numerical and experimental results of Calvetti and Di prisco (2012) for (a) maximum impact force (F^{max}_{boul}) and (b) maximum penetration depth (Z^{max}_{boul}) at equivalent falling height (h_f).

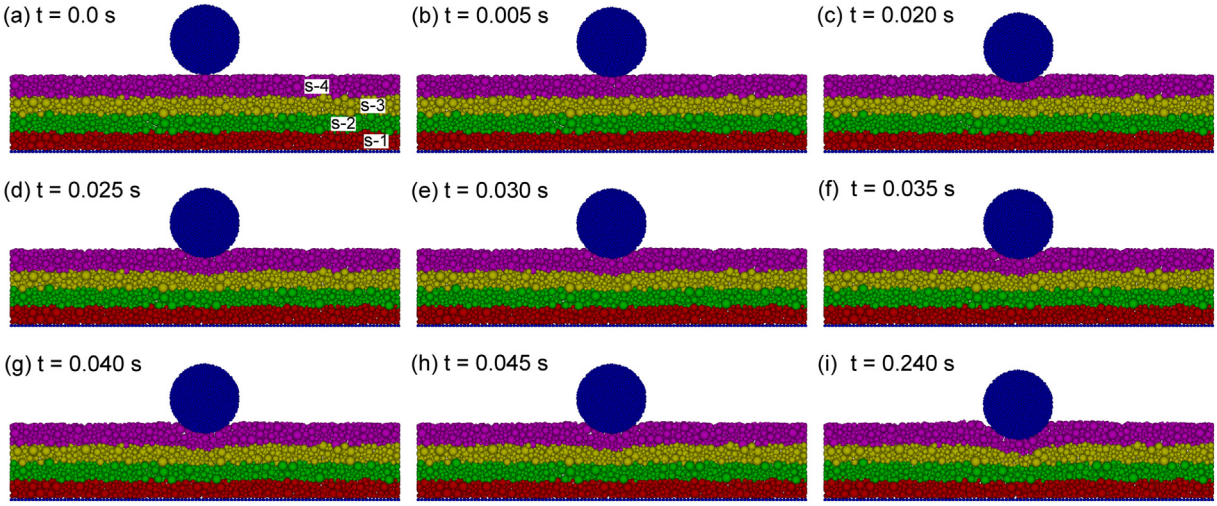

Fig. 5. Dynamic interactions between the rock block (B-1) and the granular soil layer during a simulation of h_f = 11.5 m.

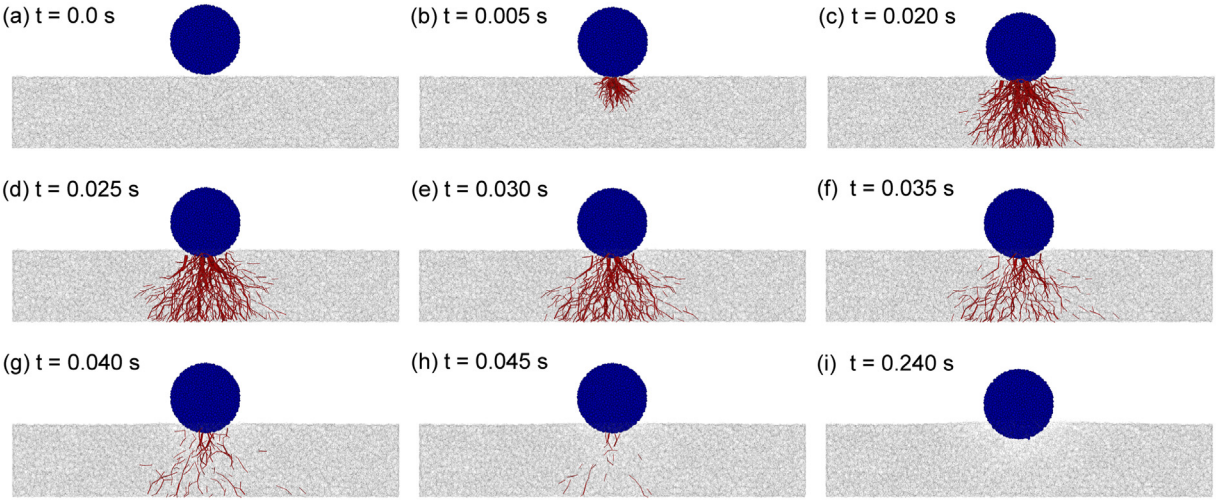

Fig. 6. Evolution of contact force chains during rockfall impact (the rock block is B-1, h_f = 11.5 m). The thickness of force chains is proportional to the force magnitude, and red if force is larger than 7500 N, otherwise gray. Note that the threshold value (7500 N) is the largest contact force at t = 0.0 s. (For interpretation of the references to colour in this figure legend, the reader is referred to the web version of this article.)

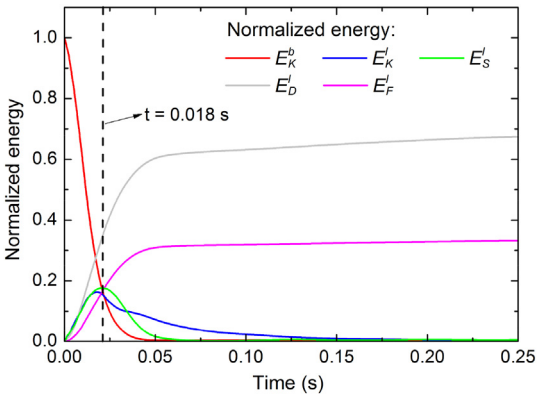

Fig. 7. Evolution of normalized kinetic energy of the rock block (B-1) during a simulation of h_f = 11.5 m. The energy components are normalized by the initial kinetic energy of rock block.

propagations. According to Zhang et al. (2017b), this is induced by the formation of force chains in the soil layer. The existence of these force chains also indicates that abundant strain energy has been stored at the contacts of soil particles. After t = 0.018 s, the kinetic energy of soil particles decreases gradually to zero, while E_F^l and E_D^l increase slowly to the peak and stable values of 0.32 and 0.68, respectively. The strain energy of the soil particles decreases quickly to zero as the force chains vanish (see Fig. 6 (d)-(h)). According to Fig. 7, it can also be observed that a major portion of impact energy has been dissipated by friction and damping forces between soil particles. In particular, the particle damping in soil layer plays a dominant role in this process.

3.3. Influence of rock block shape on impact force

Fig. 8 presents the evolution of impact force (F_{boul}) acting on rock blocks with various shapes (i.e. B-1, B-2, B-3 and B-4) falling from four different equivalent heights (i.e. h_f = 5.1, 11.5, 20.4 and 45.9 m). After impact, the impact force firstly increases quickly to the peak value within a short time period, and then decreases gradually to zero. As expected, the results show an increase of the maximum impact force with the equivalent falling height, due to the increasing kinetic energy at impact. At a given falling height, the maximum impact force increases with the block sphericity. The tests B-3 and B-4 exhibit intense oscillations of the post-peak impact force, while blocks with high sphericity (e.g. B-1 and B-2) exhibit smooth impact force curves. This phenomenon is related to the formation and vanishing of force chains

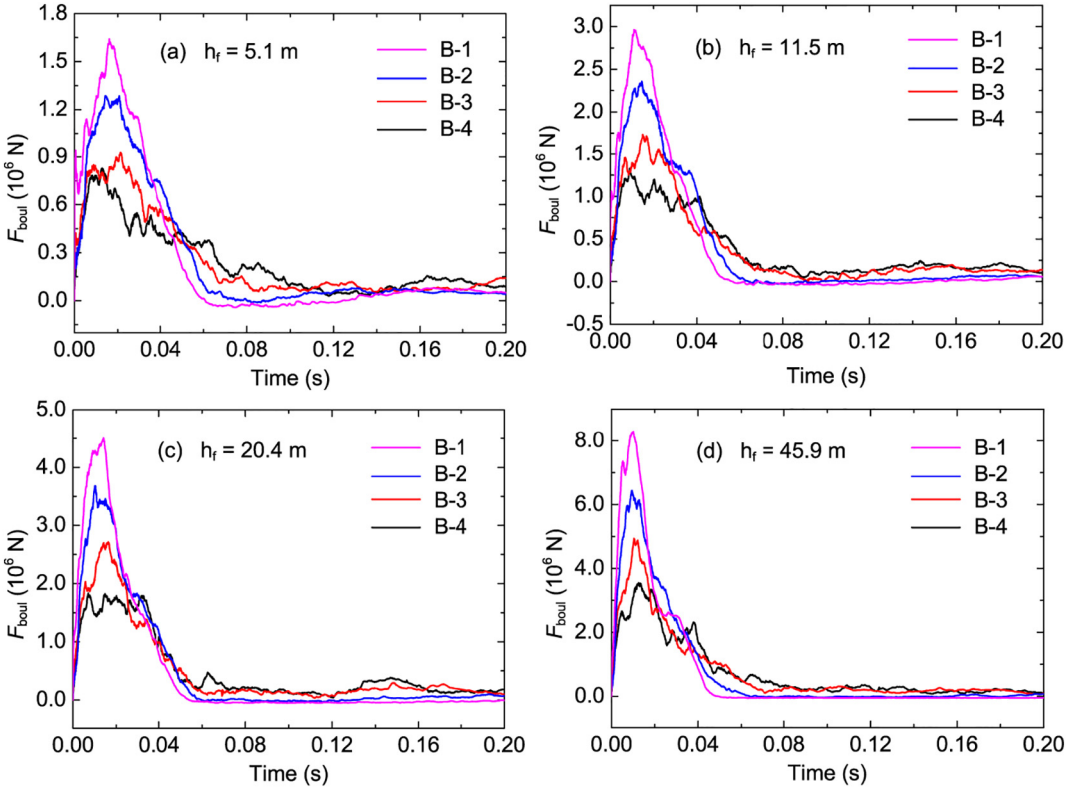

Fig. 8. Evolution of the impact force (F_{boul}) for rock blocks (B-1, B-2, B-3 and B-4) falling from four equivalent heights: (a) h_f = 5.1 m, (b) h_f = 11.5 m, (c) h_f = 20.4 m, and (d) h_f = 45.9.

near the impacting area in the soil buffering layer. Since rock blocks of low sphericity have relatively small contact surface areas to the soil buffering layer, the number of block-particle contacts is small. Thus, the formation/vanishing of individual force chain can significantly influence the total force acting on the rock block, resulting in intense oscillations. On contrary, the blocks of high sphericity can have more contacts with the soil particles, leading to large impact forces and low oscillations. In addition, soil particles are less likely to be pushed laterally for rock blocks with high sphericity due to lateral confinement imposed by other stressed particles. Consequently, the force chains in the soil buffering layer can remain stable at interactions with the rock block.

Fig. 9 presents the relationship between the maximum impact force (F_{boul}^{max}) and the block sphericity (S_p) for tests with different falling heights. It can be seen that for a specific value of S_p, the impact force

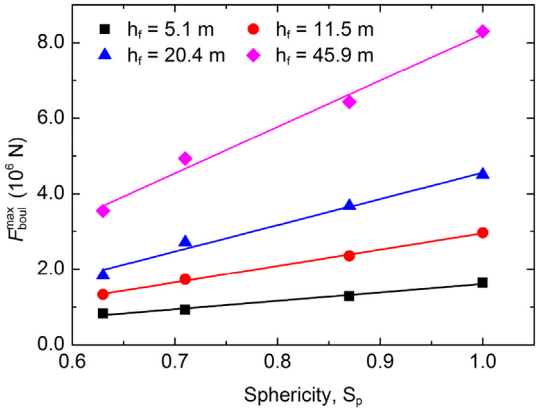

Fig. 9. Relationship between the maximum impact force (F_{boul}^{max}) and the block sphericity (S_p) for tests of various equivalent falling heights (h_f).

increases with the falling height due to the increased impact kinetic energy. For different tests, the maximum impact force increases almost linearly with S_p. The increasing rate (the slope of line) increases with the falling height. For h_f = 5.1 m, the increasing rate is 2.19 × 10^6 N, while it becomes 1.28 × 10^7 N for tests of h_f = 45.9 m. The current numerical results illustrate that the block shape can influence the block impact force significantly, especially for high speed impacts.

3.4. Impact-induced bottom force

Fig. 10 shows the evolution of bottom forces (F_{bott}) for tests with different block shapes and equivalent falling heights. For all tests, the increase of F_{bott} starts from 0.01 s when the stress wave propagates to the bottom (see the discussion on Fig. 3(a)). This time delay appears to be an intrinsic property of soil buffering layer and be independent of block shape and falling height. During impact, F_{bott} firstly increases quickly to the peak value, and then decreases to be negative. Such phenomenon has also been observed by Calvetti and di Prisco (2012) in large scale rockfall impact experiments. According to their interpretations, the decrease of bottom force is due to temporary separation (rebound) of soil particles from the bottom floor. As shown in Fig. 10, both the peak positive and negative values of bottom force increase with the block sphericity, indicating that blocks of high sphericity can transfer more strong force waves (or impact energy) to the bottom floor. The increased negative bottom force also indicates that the local soil particles have a high potential to bounce up during the impact (see discussions on Fig. 3(a)). The subsequent penetration of rock block into the soil buffering layer causes a long period of bottom force oscillations.

The maximum positive bottom force (F_{bott}^{max}) for tests on different blocks (S_p) are summarized in Fig. 11. According to the figure, F_{bott}^{max} increases with the equivalent falling height, which is in accordance with the increasing pattern of the maximum impact force. At a given falling height, F_{bott}^{max} increases linearly with the block sphericity. The increasing rate (e.g. slope of the straight line) increases slightly with the

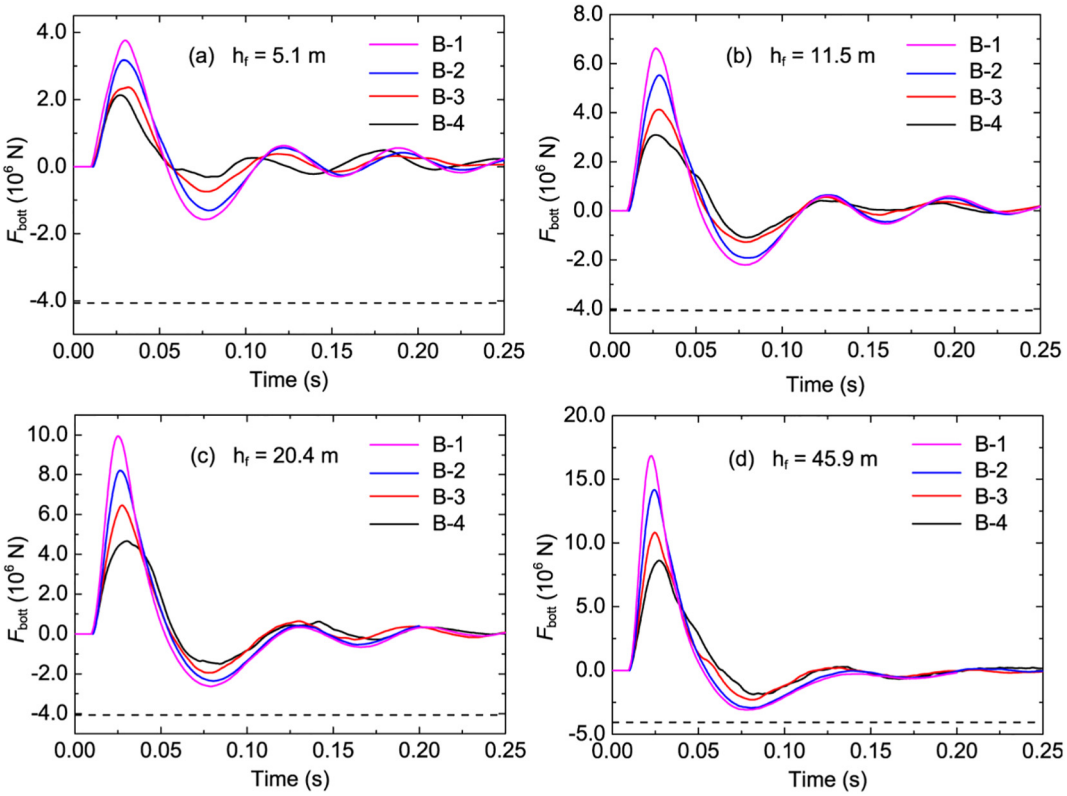

Fig. 10. Evolution of the bottom forces (F_{bott}) for four rock blocks (i.e. B-1, B-2, B-3 and B-4) impacting at four falling heights: (a) h_f = 5.1 m, (b) h_f = 11.5 m, (c) h_f = 20.4 m, and (d) h_f = 45.9 m. The dashed line in each plot denotes the critical bottom force (-4.1×10^6 N) at a state of complete separation of soil buffering layer from the bottom floor.

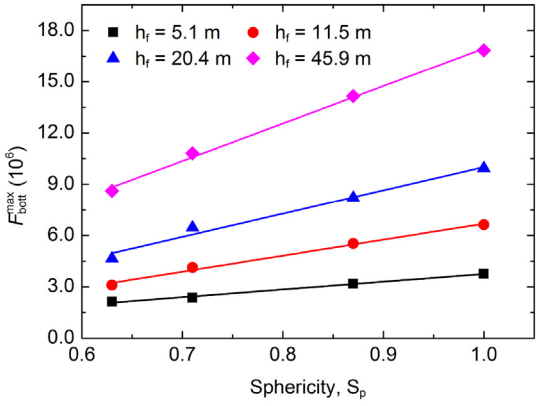

Fig. 11. Relationship between the maximum bottom force (F_{bott}^{max}) and the block sphericity (S_p) for tests using various equivalent falling heights (h_f).

falling height, showing that the influence of block shape on the maximum bottom force is significant for high speed rockfall impacts (at large falling height).

By comparing Fig. 8 and Fig. 10, it can be seen that the peak bottom force (F_{bott}^{max}) is much larger than the peak impact force on a rock block (F_{boul}^{max}). This phenomenon is the so-called dynamic amplification effect of soil buffering layer that the maximum bottom force is much larger than the corresponding peak impact force acting on the rock block (Calvetti et al., 2005). In the present study, the maximum bottom (F_{bott}^{max}) and impact (F_{boul}^{max}) forces are summarized for various tests, while their ratios are analyzed with respect to the block sphericity, as shown in Fig. 12. According to Fig. 12(a), F_{bott}^{max} and F_{boul}^{max} are approximately linearly correlated and the slope of the fitting line is between 2.0 and 3.0, with most of the data close to 2.0. This value is comparable with the experimental result of 2.0 reported in Stoffel (1998) and the numerical result of 2.1 reported in Zhang et al. (2017a), even though different testing conditions have been employed in the experiments and DEM simulations. This slope is defined as the dynamic amplification ratio (α) which has been widely used to estimate the maximum bottom force when the impact force on the rock block is known (*Ministry of Transport of the People's Republic of China*, 1995; Japan Road Association, 2000; ASTRA, 2008). In fact, the amplification ratio has been widely used to estimate the bottom force actingon geo-structures for engineering designs, with incomplete considerations of block shape and impact velocity effects.

Fig. 12 (b) shows the dependence of α on the block sphericity. It can be seen that at a given falling height, the amplification ratio decreases with the block sphericity. An increase of block sphericity from 0.63 to 1.0 can lead to 12% ~ 20% decrease of the amplification ratio. In particular, the fast impact of a spherical block (S_p = 1.0) can lead to an amplification ratio close to 2.0, which matches well the experimental observations (Stoffel, 1998; Schellenberg, 2008) on impacts by a sphere or cylinder. Thus, it is reasonable to conclude that the amplification ratio of rock block impact depends mainly on the block shape. In addition, the dynamic amplification ratio curve at low impact velocity (e.g. h_f = 5.1 m, 11.5 m) exhibits a convex shape, whereas it becomes concave at high impact velocity (e.g. h_f = 20.4 m, 45.9 m). This phenomenon illustrates that the block shape effect can be dominant at high speed impact.

3.5. Bottom stress distribution

To analyze the distribution of normal stress, the bottom floor has been divided into 11 × 11 mesh grids (see the inset plot of Fig. 13 (a)). The normal stress (σ_r) at a given radial distance (r) from the center of bottom is calculated as the average stress acting on mesh cells located at the four quadrantal cells as,

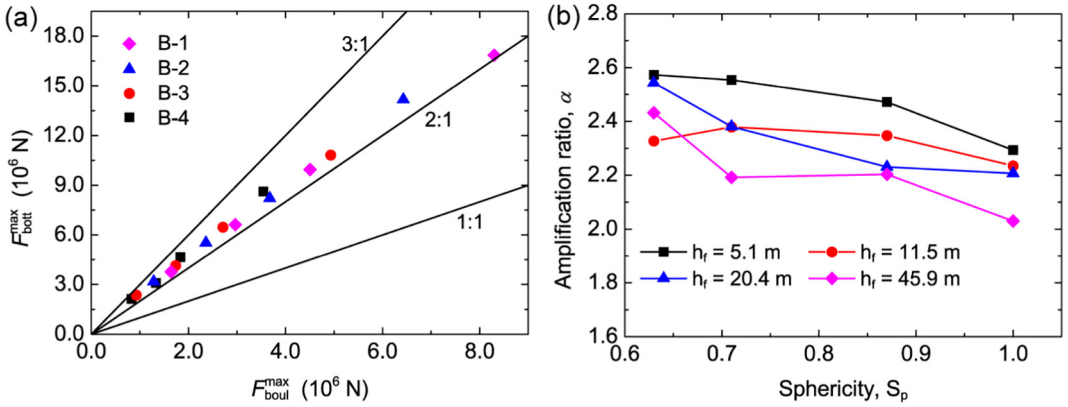

Fig. 12. (a) Relationship between the maximum bottom force and maximum impact force; (b) dependence of the dynamic amplification ratio on the block sphericity.

$$\sigma_r = \sum_{i=1}^{4} \frac{F_i^r}{S_i}/4 \tag{16}$$

where F_i^r is the summation of normal contact forces at the i-th mesh cell with a radial distance of r from the center of bottom; S_i is the area of the i-th mesh cell. Note that the center of bottom locates just vertically under the impact point.

The value of σ_r evolves with time during the rockfall impact and the maximum value is denoted as σ_r^{max}. Fig. 13 summarizes the distribution of σ_r^{max} at various radial distances (r) for different tests. As expected, σ_r^{max} at any location increases with the block falling height regardless of the block sphericity. For a given falling height and radial distance, the maximum stress increases with the block sphericity, which is in accordance with the dependence of impact and bottom forces on the block sphericity. The increasing trend of σ_r^{max} with the block sphericity becomes gradually evident as the falling height increases (see Fig. 13(c)-(d)). However, it is observed that for all tests, the block shape has little influence on the general distribution pattern of σ_r^{max} on the bottom floor. The calculated peak normal stress occurs just underneath the impacting point, and σ_r^{max} decreases with the radial distance. The vertical stress at the outer perimeter of the bottom ($r \geq 4.0$ m) decreases by at least 95% when compared to the maximum stress at the center ($r = 0$ m). The numerical results can be fitted by a unique peak function of a general form as,

$$\sigma_r^{max} = a + \frac{b-a}{1 + 10^{(\mathrm{Log}r_0 - r)c}} \tag{17}$$

where a and b are the bottom and top asymptote of fitting function, respectively; r_0 being the center of function; c being the slope of function at $r = r_0$.

It is worth to note that the fitting of DEM results by Eq. (17) in Fig. 13 has a high accuracy ($R^2 = 0.98$), which illustrates the reliability

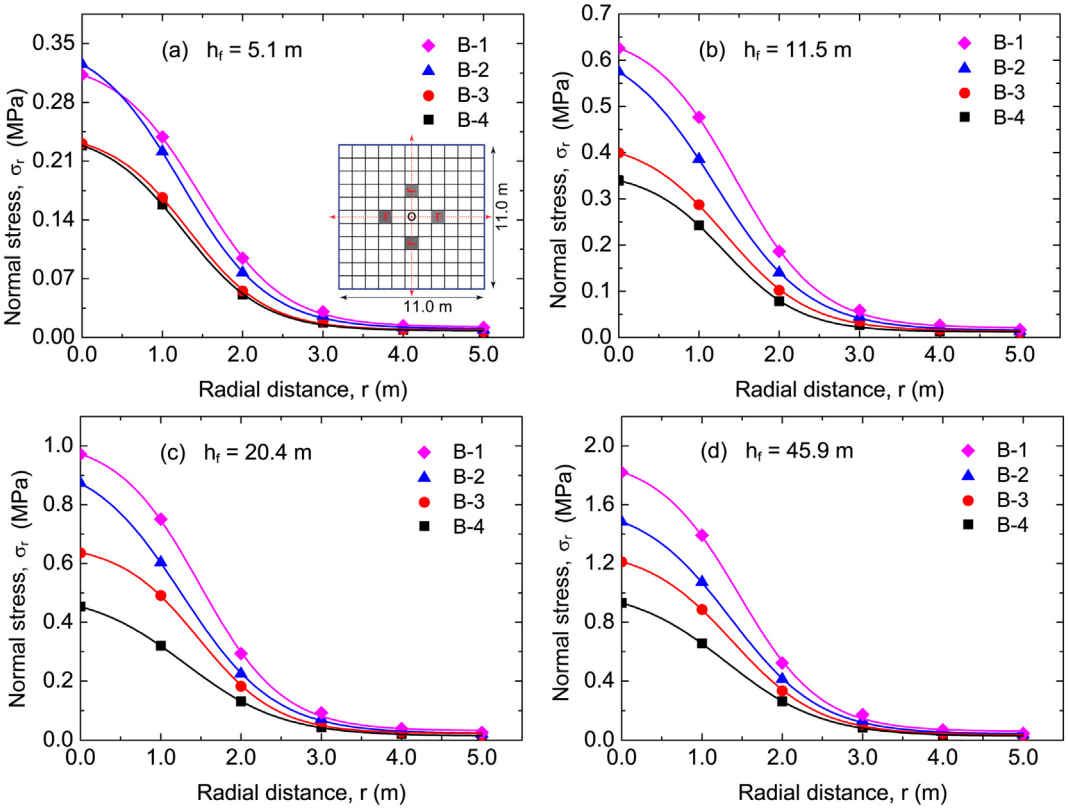

Fig. 13. Distribution of peak normal stress at the bottom as a function of radial distance from the center of the bottom for different tests (i.e B-1, B-2, B-3 and B-4) at the falling heights: (a) h_f = 5.1 m, (b) h_f = 11.5 m, (c) h_f = 20.4 m and (d) h_f = 45.9 m. The inset plot in (a) shows the bottom mesh grids.

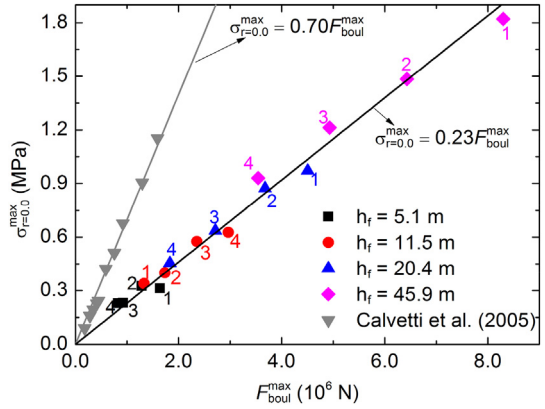

Fig. 14. Relationship between the maximum stress acting on the bottom center (r = 0.0 m) and the maximum impact force on the block. The index 1, 2, 3 and 4 represent numerical results for the rock block type B-1, B-2, B-3 and B-4, respectively.

of using this function to describe the general trend of normal stress distribution at the bottom. The general trend of fitting curve could be governed by the block shape, e.g. axial symmetry and circular cross section area.

According to Calvetti and di Prisco (2012), the progressive propagation of impact force wave from the soil surface to the bottom can be illustrated effectively by the relationship between the maximum impact force (F^{max}_{boul}) and the maximum stress ($\sigma^{max}_{r=0.0}$) at r = 0.0 m. Fig. 14 shows the dependence of $\sigma^{max}_{r=0.0}$ on F^{max}_{boul} for rock blocks falling from different heights. The maximum stress at r = 0.0 m increases linearly with the maximum impact force and the slope of the fitting line is 0.23. This indicates that a unique ratio of $\sigma^{max}_{r=0.0}$ to F^{max}_{boul} exists which is independent of the block sphericity and falling height. Such a linearly correlating pattern is in agreement with the experimental results reported in Calvetti et al. (2005), even though the testing materials are different. The ratio obtained in Calvetti et al. (2005) is 0.70 which is larger than that obtained in this study. The difference could be caused by the different thickness and material properties of the granular soil.

3.6. Maximum penetration depth

In engineering design, the maximum penetration depth (Z^{max}_{boul}) of a rock block into a soil buffering layer is also an important parameter to be considered (Pichler et al., 2005; di Prisco and Vecchiotti, 2010). Fig. 15 illustrates the dependence of maximum penetration depth on the block sphericity for tests of various falling heights. As expected, tests on rock blocks of the same sphericity exhibit increasing maximum

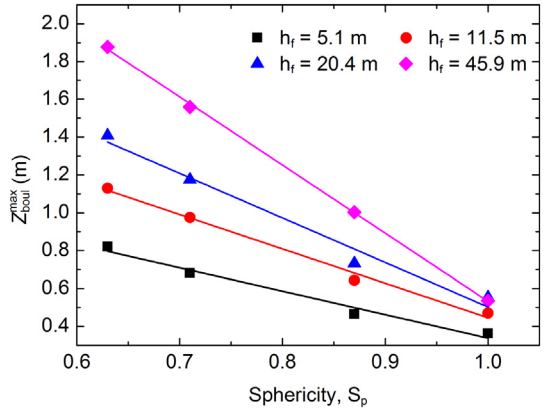

Fig. 15. Relationship between the maximum penetration depth ($Z_{boul}{}^{max}$) and the block sphericity (S_p) for tests of various equivalent falling heights (h_f).

penetration depth with the equivalent falling height. At a given falling height, the maximum penetration depth decreases linearly as the block sphericity increases. This is in agreement with the conclusions reached in Breugnot et al. (2016) and Degago et al. (2008) that the corner impact of a cubic rock block (i.e. low sphericity) is more penetrable than the sphere impact. According to the description on Fig. 8, the impact induced force chains beneath rock blocks of low sphericity can form/vanish quickly due to very small impact areas, exhibiting a more penetrable behavior. From Fig. 15, it also can be seen that the decreasing rate (the slope of the fitting line) increases with the equivalent falling height, indicating that the influence of block sphericity on the penetration depth becomes increasingly significant for high speed impacts.

4. Discussion

The current numerical analyses of rockfall impact illustrate that the rock block shape is an important factor to be considered in designing soil buffering layers for concrete/rock sheds. In the analyses, three important parameters affected by the block shape are noteworthy: the maximum impact force, maximum bottom force and maximum penetration depth. In engineering design, the maximum impact force is usually estimated by some empirical formula such as design codes used in different countries. Several other formulas have also been proposed in some well-documented publications to calculate the maximum forces by falling weights tests (Labiouse et al., 1996; di Prisco and Vecchiotti, 2006; di Prisco and Vecchiotti, 2010). In these studies, the shape of impact rock block is consistently assumed to be spherical. However, the numerical results in this study indicate that the maximum impact force increases with the sphericity of rock blocks (see Fig. 9). As a result, the maximum impact force is overestimated by these formulas. In addition, the maximum bottom force estimated by multiplying the maximum impact force with the amplification coefficient in engineering design is also very conservative if the rock block shape is simplified as spherical. Therefore, for designing effective and economical concrete/rock sheds, the rock block shape effect should be considered.

The numerical results also indicate that the maximum penetration depth decreases with the sphericity of rock block (see Fig. 15). This effect becomes very significant at high speed impact. Hence, it can be concluded that the maximum penetration depth could be underestimated if the spherical rock block is used in the analyses. In fact, rock blocks with low sphericity can penetrate easily the soil buffering layer, creating potential damage to the substrate concrete/rock shed (Schellenberg, 2008; Yan et al., 2018). According to Yu et al. (2018), if the rock block penetrates through the soil buffering layer and reach the bottom, the impact force can increase sharply because of the high rigidity of concrete/rock sheds. Therefore, in preliminary designs of rock sheds, the influence of rock block shape on the maximum penetration depth should be considered carefully to identify an effective thickness of a soil buffering layer.

5. Conclusions

The impact of rockfall against a soil buffering layer on a concrete/rock shed has been analyzed via the discrete element method. This model was validated by comparing the numerical results with some well-documented numerical and experimental data reported in the literature. The validated model was then used to investigate the influence of rock block shape on the mechanical response of rockfall impact.

In this study, the falling rock blocks are geneated as ellipsoids of the same mass but different volume (i.e. different particle density). A series of simulations on a range of block sphericity and equivalent falling heights have been conducted. The sudden impact of a rock block onto a soil buffering layer generates a series of contact force waves spreading radially from the impact point down into the substrate soil buffering layer. The strong contact forces concentrate mainly underneath the rock block, while the small contact forces distribute to the propagating front

in the soil buffering layer. The force chains firstly approach the bottom floor and then spread laterally. The force chains vanish as the impact force decreases gradually. The maximum impact and bottom forces increase, while the maximum penetration depth decreases linearly with the block sphericity. These linear relationships show the potential of using block sphericity as an index to analyze the behavior of rockfall impact. The numerical results also indicate that the rock block shape has little influence on the stress amplification of the soil buffering layer and the peak stress distribution on the bottom floor. The peak stress at the bottom center exhibits a linear dependence on the maximum impact force. The presented numerical findings are useful for the design of effective and economical concrete/rock sheds where granular soil is used as the buffering material.

Acknowledgements

This research was supported by National Key R&D Program of China (grant 2017YFC1502504), the National Natural Science Foundation of China (grant 51639008, 41602289) and the Fundamental Research Funds for the Central Universities (grant 2017SCU04A09). The constructive comments by Dr. S. Lambert greatly helped in improving the manuscript.

References

Agliardi, F., Crosta, G.B., Frattini, P., 2009. Integrating rockfall risk assessment and countermeasure design by 3D modelling techniques. Nat. Hazard Earth Syst. 9 (4), 1059–1073.
ASTRA, 2008. Actions de chutes de pierres sur les galeries de protection. Office fédéral des routes OFROU.
Bourrier, F., Nicot, F., Darve, F., 2008. Physical processes within a 2D granular layer during an impact. Granul. Matter 10 (6), 415–437.
Bourrier, F., Nicot, F., Darve, F., 2010. Evolution of the micromechanical properties of impacted granular materials. Comp. Rendus Mecanique 338, 639–647.
Breugnot, A., Lambert, S., Villard, P., Gotteland, P., 2016. A discrete/continuous coupled approach for modeling impacts on cellular geostructures. Rock Mech. Rock. Eng. 49 (5), 1831–1848.
Calvetti, F., di Prisco, C., 2012. Rockfall impacts on sheltering tunnels: real-scale experiments. Geotechnique 62 (10), 865–876.
Calvetti, F., Di Prisco, C., Vecchiotti, M., 2005. Experimental and numerical study of rockfall impacts on granular soils. Riv. Ital. Geotec. 4, 95–109.
Crosta, G.B., Agliardi, F., 2004. Parametric evaluation of 3D dispersion of rockfall trajectories. Nat. Hazards Earth Syst. Sci. 4 (4), 583–598.
Cruden, D.M., Varnes, D.J., 1958. Landslide Types and Processes. Special Report - National Research Council. Transp. Res. Board 247, 20–47.
Cundall, P.A., Strack, O.D.L., 1979. A discrete numerical model for granular assemblies. Geotechnique 29 (1), 47–65.
Degago, S., Ebeltoft, R., Nordal, S., 2008. Effect of Rock fall Geometries Impacting Soil Cushion: A Numerical Procedure. In: *The 12th International Conference of International Association for Computer Methods and Advances in Geomechanics* India.
di Prisco, C., Vecchiotti, M., 2006. A rheological model for the description of boulder impacts on granular strata. Géotechnique 56 (7), 469–482.
di Prisco, C., Vecchiotti, M., 2010. Design charts for evaluating impact forces on dissipative granular soil cushions. J. Geotech. Geoenviron. Eng. 136 (11), 1529–1541.
Dorren, L.K.A., 2003. A review of rockfall mechanics and modelling approaches. Prog. Phys. Geogr. 27 (1), 69–87.
Ferrari, F., Giacomini, A., Thoeni, K., 2016. Qualitative rockfall hazard assessment: a comprehensive review of current practices. Rock Mech. Rock. Eng. 49 (7), 2865–2922.
Fityus, S.G., Giacomini, A., Buzzi, O., 2013. The significance of geology for the morphology of potentially unstable rocks. Eng. Geol. 162, 43–52.
Gao, G., Meguid, M., 2018a. Modeling the impact of a falling rock cluster on rigid structures. Int. J. Geomech. 18 (2), 1–15.
Gao, G., Meguid, M.A., 2018b. On the role of sphericity of falling rock clusters—insights from experimental and numerical investigations. Landslides 15 (2), 219–232.
Glover, J., 2015. Rock-shape and Its Role in Rockfall Dynamics. Durham University (PhD Thesis).
Glover, J., Bartelt, P., Christen, M., Gerber, W. 2015. Rockfall-Simulation with Irregular Rock Blocks. Springer International Publishing, Cham, 1729–1733.
Itasca, 2003. PFC3D: Theory and Background. Itasca Consulting Group, Inc, Minneapolis.
Japan Road Association, 2000. Manual for Anti-impact Structures Against Falling Rocks. (Japan).
Krumbein, W.C., 1941. Measurement and geological significance of shape and roundness of sedimentary particles. J. Sediment. Res. 11 (2), 64–72.
Labiouse, V., Descoeudres, F., Montani, S., 1996. Experimental study of rock sheds impacted by rock blocks. Struct. Eng. Int. 3 (3), 171–176.
Lambert, S., Bourrier, F., 2013. Design of rockfall protection embankments: a review. Eng. Geol. 154, 77–88.
Lambert, S., Gotteland, P., Nicot, F., 2009. Experimental study of the impact response of geocells as components of rockfall protection embankments. Nat. Hazard Earth Syst. 9 (2), 459–467.
Leine, R.I., Schweizer, A., Christen, M., Glover, J., Bartelt, P., Gerber, W., 2014. Simulation of rockfall trajectories with consideration of rock shape. Multibody Syst. Dynam. 32 (2), 241–271.
Ministry of Transport of the People's Republic of China. In: Specifications for Design of Highway Subgrades, (JTJ013-95).
Pichler, B., Hellmich, C., Mang, H.A., 2005. Impact of rocks onto gravel Design and evaluation of experiments. Int. J. Impact Eng. 31 (5), 559–578.
Potyondy, D.O., Cundall, P.A., 2004. A bonded-particle model for rock. Int. J. Rock Mech. Min. Sci. 41 (8), 1329–1364.
Roethlin, C., Calvetti, F., Yamaguchi, S., Vogel, T., 2013. Numerical simulation of rockfall impact on a rigid reinforced concrete slab with a cushion layer. In: *Fourth International Workshop on Performance,* Protection and Strengthening of Structures, Mysore, India.
Schellenberg, K., 2008. On the Design of Rockfall Protection Galleries. Swiss Federal Institute of Technology, Zurich (PhD Thesis).
Shen, W., Zhao, T., Zhao, J., Dai, F., Zhou, G.G.D., 2018. Quantifying the impact of dry debris flow against a rigid barrier by DEM analyses. Eng. Geol. 241, 86–96.
Stoffel, S.M., 1998. Sollicitation Dynamique de la Couverture des Galeries de Protection Lors de Chutes de Blocs. (Ph.D, EPFL (Ph.D Thesis).
Utili, S., Zhao, T., Houlsby, G.T., 2015. 3D DEM investigation of granular column collapse: evaluation of debris motion and its destructive power. Eng. Geol. 186, 3–16.
Valagussa, A., Frattini, P., Crosta, G.B., 2014. Earthquake-induced rockfall hazard zoning. Eng. Geol. 182, 213–225.
Volkwein, A., Schellenberg, K., Labiouse, V., Agliardi, F., Berger, F., Bourrier, F., Dorren, L., Gerber, W., Jaboyedoff, M., 2011. Rockfall characterisation and structural protection – a review. Nat. Hazard Earth Syst. 11 (9), 2617–2651.
Wang, Y., 2009. A new algorithm to model the dynamics of 3-D bonded rigid bodies with rotations. Acta Geotech. 4 (2), 117–127.
Wang, Y., Mora, P., 2009. The ESyS_Particle: A New 3-D Discrete Element Model with Single Particle Rotation. Advances in Geocomputing. Springer Berlin Heidelberg, Berlin, Heidelberg, pp. 183–228.
Weatherley, D., Hancock, W., Boris, V., 2014. ESyS-Particle Tutorial and User's Guide Version 2.1. Earth Systems Science Computational Centre, The University of Queensland.
Yan, P., Zhang, J., Fang, Q., Zhang, Y., 2018. Numerical simulation of the effects of falling rock's shape and impact pose on impact force and response of RC slabs. Constr. Build. Mater. 160, 497–504.
Yu, B., Yi, W., Zhao, H., 2018. Experimental study on the maximum impact force by rock fall. Landslides 15 (2), 233–242.
Zhang, L., Lambert, S., Nicot, F., 2017a. Discrete dynamic modelling of the mechanical behaviour of a granular soil. Int. J. Impact Eng. 103, 76–89.
Zhang, L., Nguyen, N.G.H., Lambert, S., Nicot, F., Prunier, F., Djeran-Maigre, I., 2017b. The role of force chains in granular materials: from statics to dynamics. Eur. J. Environ. Civil Eng. 21 (7–8), 874–895.
Zhao, T., Dai, F., Xu, N., 2017. Coupled DEM-CFD investigation on the formation of landslide dams in narrow rivers. Landslides 14 (1), 189–201.
Zhao, T., Crosta, G., Dattola, G., Utili, S., 2018. Dynamic fragmentation of jointed rock blocks during rockslide-avalanches: insights from discrete element analyses. J. Geophys. Res. Sol. Earth 123, 1–20.